Positron collisions with acetylene calculated using the *R*-matrix with pseudo-states method

2011 J. Phys. B: At. Mol. Opt. Phys. 44 195203

(http://iopscience.iop.org/0953-4075/44/19/195203)

J. Phys. B: At. Mol. Opt. Phys. **44** (2011) 195203 (9pp) doi:10.1088/0953-4075/44/19/195203

Positron collisions with acetylene calculated using the *R*-matrix with pseudo-states method

Rui Zhang, Pavlos G Galiatsatos and Jonathan Tennyson

Department of Physics and Astronomy, University College London, Gower St., London WC1E 6BT, UK

E-mail: j.tennyson@ucl.ac.uk

Received 22 June 2011, in final form 8 August 2011
Published 13 September 2011
Online at stacks.iop.org/JPhysB/44/195203

Abstract

Eigenphase sums, total cross sections and differential cross sections are calculated for low-energy collisions of positrons with C_2H_2. The calculations demonstrate that the use of appropriate pseudo-state expansions very significantly improves the representation of this process giving both realistic eigenphases and cross sections. Differential cross sections are strongly forward peaked in agreement with the measurements. These calculations are computationally very demanding; even with improved procedures for matrix diagonalization, fully converged calculations are too expensive with current computer resources. Nonetheless, the calculations show clear evidence for the formation of a virtual state but no indication that acetylene actually binds a positron at its equilibrium geometry.

(Some figures in this article are in colour only in the electronic version)

1. Introduction

Despite the absence of exchange interactions, low-energy positron collisions with molecules are much more difficult to represent using *ab initio* methods than the better studied electron–molecule collision problem. This is because the Coulomb attraction between a scattering positron and the target electrons is hard to model using standard coordinate systems. However, the electron–positron correlation gives rise to effects variously known as polarization and virtual positronium formation which are vital for an accurate representation of low-energy scattering problems. This means that, for instance, standard close-coupling expansions which are widely used to successfully represent low-energy electron–molecule collisions (Tennyson 2010) give poor results for the positronic counterparts (Tennyson 1986, Danby and Tennyson 1991).

Recently, we reported calculations for collisions of low-energy positrons with molecular hydrogen using the molecular *R*-matrix with pseudo-states (MRMPS) method (Zhang *et al* 2011). These calculations gave excellent results for elastic cross sections and eigenphases at energies below the positronium formation threshold and wavefunctions. Furthermore, use of these wavefunctions to calculate the effective number of target electrons available for annihilation, $Z_{\rm eff}$, gave a much better representation of positron–electron cusp than previous studies which did not explicitly include the positron–electron distance in the wavefunction.

It is obviously encouraging that the MRMPS method gives good results for the e^+–H_2 problem, but H_2 is a simple enough target for specially adapted methods to be used. A number of these specialist calculations give excellent results for this system (Armour *et al* 1990, Cooper *et al* 2008, Zhang *et al* 2009). A more demanding test is, therefore, to consider positron collisions with a many-electron target for which these specialized methods are not applicable. In this paper, we consider the altogether more challenging problem of low-energy e^+–C_2H_2 collisions.

Acetylene provides a particularly suitable example since it is the smallest of a number of organic molecules whose measured $Z_{\rm eff}$ values are much larger than Z, the actual number of target electrons (Gribakin *et al* 2010). For the acetylene molecule, $Z_{\rm eff} = 3160$ (Barnes *et al* 2003) and $Z = 14$. This phenomenon is assumed to be due to the formation of a pseudo-bound positron–molecule state (Paul and Saint-Pierr 1963, Gribakin *et al* 2010), although in the actual case of acetylene it has been suggested that the annihilation actually proceeds via the formation of a virtual state (Nishimura and Gianturco 2003).

Calculated integral cross sections and differential cross sections for positron collisions with C_2H_2 using the *R*-matrix method have been performed with the static model and static plus polarization model by Franz *et al* (2008). These authors also gave both integral and differential cross sections computed using semi-empirical procedures based on density functional theory (DFT) and the distributed positron model (DPM), as well as a semi-empirical *R*-matrix calculation in which the electron–positron attraction was arbitrarily enhanced. Cross sections for positron–C_2H_2 collision have also been calculated by several groups (da Silva *et al* 1998, de Carvalho *et al* 2000a, 2000b, Nishimura and Gianturco 2005). Total elastic scattering cross sections were measured by Sueoka and Mori (1989) for positron collisions with acetylene at incident energies between 1 and 400 eV. Measured, relative elastic differential cross sections (DCSs) were reported by Kauppila *et al* (2002) at 4, 6.75, 10, 20, 50 and 100 eV.

Here, we present a study of positron collisions with the acetylene molecule. Calculations are performed at different levels: static, static plus polarization and close coupling using the MRMPS method. Within the MRMPS method, our calculations are carried out for several models. While none of our calculations give evidence for a true bound state of e^+–C_2H_2, we analyse the possible existence of a virtual state by calculating the scattering length based on the s-wave eigenphase.

2. Method

2.1. *R*-matrix with pseudo-states method

For a positron–molecule collision, the close-coupling expansion can be written as

$$\psi_k^{N+1} = \sum_{ij} a_{ijk} \Phi_i^N(\mathbf{x}_1, \mathbf{x}_2, ..., \mathbf{x}_N) u_{ij}(\tilde{\mathbf{x}}) + \sum_i b_{ik} \chi_i^{N+1}(\mathbf{x}_1, \mathbf{x}_2, ..., \mathbf{x}_N, \tilde{\mathbf{x}}), \quad (1)$$

where Φ_i^N is the *N*-electron target wavefunction and u_{ij} are continuum orbitals carrying the positron, whose coordinate is denoted by $\tilde{\mathbf{x}}$. The second sum in equation (1) contains L^2 functions in which the positron occupies short-range target orbitals. In a calculation, as here, where a common set of orbitals are used both for the positron and the electrons, the positron is free to enter orbitals already fully occupied by electrons.

In the *R*-matrix method, this expansion is used to represent the scattering wavefunction within a sphere of radius a, outside which the target wavefunction is assumed to have zero amplitude. The outer region problem is solved in a potential given by the target moments by propagating the *R*-matrix and matching to asymptotic solutions (Tennyson 2010).

The *R*-matrix with pseudo-states (RMPS) method was originally developed by Bartschat *et al* (1996) to treat problems involving electron–atom collisions at intermediate energy. The method was adapted for similar electron–molecule problems, but there has been a growing realization that for these problems the method is most useful for converging polarization effects in low-energy electron–molecule collisions (Halmová and Tennyson 2008, Halmová *et al* 2008, Tarana and Tennyson 2008). Indeed, MRMPS expansions have been demonstrated to give a good representation of the target polarizability (Jones and Tennyson 2010), a property that can be used as a proxy for determining the convergence of the representation of polarization in a collision.

The basic equation of the MRMPS method is still equation (1), but involves a generalization of the target wavefunction Φ_i^N; the sum i runs over not only a set of wavefunctions designed to represent low-lying electronically excited states of the target but also over a series of pseudo-states which are designed to represent, within the *R*-matrix sphere, both the neglected, higher-lying target states and the target continuum. In the MRMPS method, this is achieved by using a set of n even-tempered Gaussian type orbitals (GTOs) for each ℓ. These functions have exponents defined by

$$\alpha_i = \alpha_0 \beta^{(i-1)}, \qquad i = 1, \ldots, n. \quad (2)$$

These extra GTOs, which once orthogonalized to the target orbitals, we refer to as pseudo-continuum orbitals or PCOs below, are used to represent one-electron excitations of the target wavefunction. For positron collisions it is only necessary to consider excitations which have the same spin symmetry as the target ground state. However, our study on e^+–H_2 showed that for positron collisions the PCO basis converges slowly with respect to the ℓ, the angular momentum of the functions included in the PCO expansion (Zhang *et al* 2011).

Thus far, the most successful MRMPS calculations have concentrated on problems with two active target electrons (Gorfinkiel and Tennyson 2004, 2005, Tarana and Tennyson 2008, Zhang *et al* 2011). For many electron problems there is some flexibility on the choice of the MRMPS model (Halmová *et al* 2008) and, more seriously, a rapidly increasing computational cost as the number of electrons considered for excitation is increased. Both of these issues are discussed further below.

2.2. Computational implementation

In the standard *R*-matrix method, all inner region wavefunctions, as represented by equation (1), are used to construct the *R*-matrix on the boundary (Burke and Berrington 1993). However, for very large calculations this method rapidly becomes impractical. To circumvent this problem Tennyson (2004) developed a version of the partitioned *R*-matrix method which allows the *R*-matrix to be constructed on the boundary using only the M lowest solutions plus appropriate correction terms. Although M is still fairly large, typically a few thousands, this still represents a very substantial computational saving for the problems considered below.

Even with the use of the partitioned *R*-matrix method, diagonalization of the scattering Hamiltonian represents the computational bottleneck in the MRMPS calculations presented here. We wish to obtain the M lowest eigenvalues and eigenvectors for an L-dimensional Hamiltonian matrix under the conditions that $M \ll L$. In practice, we wish to consider $L \geqslant 500\,000$ and $M \approx 3000$.

To keep this problem tractable, we have developed a tailored diagonalization algorithm. For this algorithm it is important to appreciate the structure of the scattering Hamiltonian (Tennyson 1996). Equation (1) shows that the Hamiltonian matrix can be divided into three parts: a block representing target wavefunction times continuum orbital function, a block representing the L^2 functions and two symmetry-related, off-diagonal blocks representing the interaction between the two types of wavefunctions. The target times continuum block is dense and of dimension approximately M. For very large problems, this block forms an increasingly small proportion of the problem. Conversely, the L^2 block is sparse and becomes increasingly sparse, due to Slater's rules, as the size of the problem increases.

Our Hamiltonian construction code SCATCI (Tennyson 1996) writes symmetry unique, non-zero matrix elements to the disk. For the larger problems considered here these comprise only about 0.3% of the total matrix, i.e. the Hamiltonian matrix is about 99.4% sparse. To diagonalize the Hamiltonian matrix, **H**, we have developed a highly optimized and parallelized version of the iterative diagonalizer ARPACK (Lehoucq *et al* 1998) to obtain the lowest M roots. From a computational perspective, ARPACK has two basic steps. Like most iterative diagonalizers, the matrix is sampled using an image vector, **x**, via the matrix–vector multiplication

$$\boldsymbol{y} = \mathbf{H}\mathbf{x}. \tag{3}$$

For this step, a special sparse matrix–vector product (SMVP) routine was used. More specifically, the Hamiltonian matrix elements are read from disk and stored in RAM in a local variation of the official coordinate sparse matrix format. Then using the directive-based language OpenMP (www.openmp.org), we developed a parallel SMVP for shared memory machines. This scales almost perfectly. When requesting only few eigenpairs, this SMVP dominates the computer usage. However, given the relatively large number of eigenpairs required, this is not the case here. The second computationally important step consists of the Schmidt orthogonalization of the Ritz vectors comprising the Krylov space (KS) plus the update process of the KS. In our case, due to RAM limitations we used a small KS fixed to 2*M vectors. The usage of a small KS results in many updates of it (64 in our case). The second step proved to be nine times more time consuming than the SMVP step. With the above configuration and using optimized and parallelized versions of basis linear algebra subroutines and LAPACK routines (see www.netlib.org/lapack) we developed a highly optimized hybrid ARPACK plus OpenMP static library.

Using the above library, we were able to obtain $M = 3000$ eigenpairs for a matrix of dimension $L = 512\,298$, consisting of 866 812 269 non-zero elements, in 27 days using an 8-shared memory core workstation and 45 GB of RAM. The total number of SMVPs is equal to the total number of Schmidt orthogonalizations. So we reorthogonalized 110 482 times 6000 vectors of dimension 512 298 each and updated the KS 64 times. This is why the second step dominates the computing time. The speed-up compared to running on a single core was 5.6. Using a larger KS (of dimension 20*M vectors for example) would further reduce the execution time.

2.3. Other details

All calculations were performed using the polyatomic UK molecular R-matrix codes (Morgan *et al* 1998, Tennyson 2010) as adapted to perform positron–molecule calculations (Baluja *et al* 2007). This version of the code uses GTOs to represent the three sets of inner region functions: the target basis functions, which are centred on the nuclei, and the continuum orbitals and PCOs, which are both centred on the target centre of mass. As C_2H_2 is a neutral target, continuum orbitals were generated assuming no potential function and are therefore the same as those for electron scattering with $a = 10\ a_0$ (Faure *et al* 2002).

The polyatomic UK molecular R-matrix codes only work with Abelian point groups, so all calculations were performed in D_{2h} rather than $D_{\infty h}$ symmetry. However, there is little ambiguity in translating back from the D_{2h} to the $D_{\infty h}$ representation, so we use $D_{\infty h}$ labels below.

The MRMPS calculation involves the use of three independent, but notionally complete, inner region basis sets, so care needs to be taken with the orthogonalization procedure. A combination of Schmidt followed by symmetric (or Löwden) orthogonalization first for the PCOs and then the continuum orbitals has been found to work well (Gorfinkiel and Tennyson 2005). At each symmetric orthogonalization step, functions whose eigenvalues of the overlap matrix are lower than some threshold value, δ_{thresh}, are deleted. Experience shows that it is necessary to use a higher value of δ_{thresh} for the PCOs than the continuum orbitals.

3. Target calculation

All of our calculations were carried out at the linear, symmetric equilibrium geometry of HCCH, $r_{CC} = 1.208$ Å and $r_{CH} = 1.058$ Å. The target GTO basis sets for the C and H atoms are the double-zeta plus polarization set of Dunning (1970). These give 9s 5p 1d basis for C and 5s 2p for H.

To understand how important polarization effects are for positron–C_2H_2 collisions at low energies, we performed calculations using several different models. We began from the simplest models: static and static plus polarization (SP). For these models, the target wavefunction is represented by its ground $\tilde{X}\ ^1\Sigma_g^+$ state, which has the configuration $1\sigma_g^2\ 1\sigma_u^2\ 2\sigma_g^2\ 2\sigma_u^2\ 3\sigma_g^2\ 1\pi_u^4$. For both the static and SP models, the target wavefunction was taken from a Hartree–Fock self-consistent field (SCF) calculation.

For MRMPS calculations, several models, see table 1, and PCOs basis sets were tested. In particular, detailed tests were performed for PCO basis sets defined by ($\alpha_0 = 0.16$, $\beta = 1.4$) ($\alpha_0 = 0.17$, $\beta = 1.4$) and ($\alpha_0 = 0.10$, $\beta = 1.4$) based on the spd-PCOs model, i.e. a model with $\ell = 0$, 1 and 2 functions in the PCO basis. The deletion threshold for orthogonalizing the PCOs to the SCF orbitals was set to $\delta_{\text{thresh}} = 2 \times 10^{-4}$. The energy differences between calculations with the different PCO basis sets are fairly small. The PCO basis set with $\alpha_0 = 0.17$ and $\beta = 1.4$ were used to run our target and various MRMPS scattering calculations up to $l = 4$.

C_2H_2 has 14 electrons, so the configuration interaction (CI) calculation can be very complicated. We tested different

Table 1. Target configurations for different models. N is the size of the Hamiltonian matrix with $^1A_{1g}$ ($^1\Sigma_g^+$) symmetry based on an spd-PCOs calculation; see the text for a detailed explanation of the configurations.

Model	N	Configurations
1	2739	$(1\sigma_g\ 1\sigma_u)^4\ (2\sigma_g\ 3\sigma_g\ 4\sigma_g\ 5\sigma_g\ 2\sigma_u\ 3\sigma_u\ 1\pi_u\ 1\pi_g)^{10}$
		$(1\sigma_g\ 2\sigma_g\ 3\sigma_g\ 1\sigma_u\ 2\sigma_u\ 1\pi_u)^{13}\ (\mathrm{PCOs})^1$
2	827	$(1\sigma_g\ 1\sigma_u)^4\ (2\sigma_g\ 3\sigma_g\ 4\sigma_g\ 2\sigma_u\ 3\sigma_u\ 1\pi_u\ 1\pi_g)^{10}$
		$(1\sigma_g\ 2\sigma_g\ 3\sigma_g\ 1\sigma_u\ 2\sigma_u\ 1\pi_u)^{13}\ (\mathrm{PCOs})^1$
3	122	$(1\sigma_g\ 2\sigma_g\ 3\sigma_g\ 1\sigma_u\ 2\sigma_u)^{10}\ 1\pi_u{}^3\ (4\sigma_g\ 3\sigma_u\ 1\pi_g)^1$
		$(1\sigma_g\ 2\sigma_g\ 3\sigma_g\ 1\sigma_u\ 2\sigma_u)^{10}\ 1\pi_u{}^2\ (4\sigma_g\ 3\sigma_u\ 1\pi_g)^2$
		$(1\sigma_g\ 2\sigma_g\ 3\sigma_g\ 1\sigma_u\ 2\sigma_u)^{10}\ 1\pi_u{}^3\ (\mathrm{PCOs})^1$
		$(1\sigma_g\ 2\sigma_g\ 3\sigma_g\ 1\sigma_u\ 2\sigma_u)^{10}\ 1\pi_u{}^2\ (4\sigma_g\ 3\sigma_u\ 1\pi_g)^1\ (\mathrm{PCOs})^1$
4	3415	$(1\sigma_g\ 1\sigma_u\ 2\sigma_g)^6\ 1\pi_u{}^4\ (3\sigma_g\ 4\sigma_g\ 2\sigma_u\ 3\sigma_u\ 1\pi_g)^4$
		$(1\sigma_g\ 1\sigma_u\ 2\sigma_g)^6\ 1\pi_u{}^3\ (3\sigma_g\ 4\sigma_g\ 2\sigma_u\ 3\sigma_u\ 1\pi_g)^5$
		$(1\sigma_g\ 1\sigma_u\ 2\sigma_g)^6\ 1\pi_u{}^4\ (3\sigma_g\ 4\sigma_g\ 2\sigma_u\ 3\sigma_u\ 1\pi_g)^3\ (\mathrm{PCOs})^1$
		$(1\sigma_g\ 1\sigma_u\ 2\sigma_g)^6\ 1\pi_u{}^3\ (3\sigma_g\ 4\sigma_g\ 2\sigma_u\ 3\sigma_u\ 1\pi_g)^4\ (\mathrm{PCOs})^1$
5	860	$(1\sigma_g\ 1\sigma_u)^4\ (2\sigma_g\ 3\sigma_g\ 4\sigma_g\ 2\sigma_u\ 3\sigma_u\ 1\pi_u\ 1\pi_g)^{10}$
		$(1\sigma_g\ 2\sigma_g\ 3\sigma_g\ 1\sigma_u\ 2\sigma_u)^{10}\ 1\pi_u{}^3\ (\mathrm{PCOs})^1$
		$(1\sigma_g\ 2\sigma_g\ 3\sigma_g\ 1\sigma_u\ 2\sigma_u)^{10}\ 1\pi_u{}^2\ (4\sigma_g\ 3\sigma_u\ 1\pi_g)^1\ (\mathrm{PCOs})^1$
6	1511	$(1\sigma_g\ 1\sigma_u)^4\ (2\sigma_g\ 3\sigma_g\ 4\sigma_g\ 2\sigma_u\ 3\sigma_u\ 1\pi_u\ 1\pi_g)^{10}$
		$(1\sigma_g\ 1\sigma_u)^4\ (2\sigma_g\ 3\sigma_g\ 2\sigma_u\ 1\pi_u)^9\ (\mathrm{PCOs})^1$
		$(1\sigma_g\ 1\sigma_u)^4\ (2\sigma_g\ 3\sigma_g\ 2\sigma_u\ 1\pi_u)^8\ (4\sigma_g\ 3\sigma_u\ 1\pi_g)^1\ (\mathrm{PCOs})^1$
7	3656	$(1\sigma_g\ 1\sigma_u)^4\ (2\sigma_g\ 3\sigma_g\ 4\sigma_g\ 5\sigma_g\ 2\sigma_u\ 3\sigma_u\ 1\pi_u\ 1\pi_g)^{10}$
		$(1\sigma_g\ 1\sigma_u)^4\ (2\sigma_g\ 3\sigma_g\ 2\sigma_u\ 1\pi_u)^9\ (\mathrm{PCOs})^1$
		$(1\sigma_g\ 1\sigma_u)^4\ (2\sigma_g\ 3\sigma_g\ 2\sigma_u\ 1\pi_u)^8\ (4\sigma_g\ 5\sigma_g\ 3\sigma_u\ 1\pi_g)^1\ (\mathrm{PCOs})^1$
8	6384	$(1\sigma_g\ 1\sigma_u)^4\ (2\sigma_g\ 3\sigma_g\ 4\sigma_g\ 2\sigma_u\ 3\sigma_u\ 1\pi_u\ 1\pi_g)^{10}$
		$(1\sigma_g\ 1\sigma_u)^4\ (2\sigma_g\ 3\sigma_g\ 2\sigma_u\ 1\pi_u)^9\ (\mathrm{PCOs})^1$
		$(1\sigma_g\ 1\sigma_u)^4\ (2\sigma_g\ 3\sigma_g\ 2\sigma_u\ 1\pi_u)^8\ (4\sigma_g\ 3\sigma_u\ 1\pi_g)^1\ (\mathrm{PCOs})^1$
		$(1\sigma_g\ 1\sigma_u)^4\ (2\sigma_g\ 3\sigma_g\ 2\sigma_u\ 1\pi_u)^7\ (4\sigma_g\ 3\sigma_u\ 1\pi_g)^2\ (\mathrm{PCOs})^1$
9	16112	$(1\sigma_g\ 1\sigma_u\ 2\sigma_g)^6\ (3\sigma_g\ 4\sigma_g\ 2\sigma_u\ 3\sigma_u\ 1\pi_u\ 1\pi_g)^8$
		$(1\sigma_g\ 1\sigma_u\ 2\sigma_g)^6\ (3\sigma_g\ 4\sigma_g\ 2\sigma_u\ 3\sigma_u\ 1\pi_u\ 1\pi_g)^7\ (\mathrm{PCOs})^1$
10	188924	$(1\sigma_g\ 1\sigma_u)^4\ (2\sigma_g\ 3\sigma_g\ 4\sigma_g\ 5\sigma_g\ 2\sigma_u\ 3\sigma_u\ 1\pi_u\ 1\pi_g)^{10}$
		$(1\sigma_g\ 1\sigma_u)^4\ (2\sigma_g\ 3\sigma_g\ 4\sigma_g\ 5\sigma_g\ 2\sigma_u\ 3\sigma_u\ 1\pi_u\ 1\pi_g)^9\ (\mathrm{PCOs})^1$

complete active space configuration interaction (CASCI) calculations for the target runs based on the MRMPS method. Table 1 shows the CI models tested and the dimension of the resulting ^1A_g ($^1\Sigma_g^+$) symmetry target Hamiltonians.

To understand these models, we take model 1 as an example. The first line gives the CASCI generated using only the target orbitals. The second line lists the configurations generated by occupying PCOs for an spd MRMPS basis, the full list of which is

6–22a_g 2–8b_{2u} 2–8b_{3u} 1–5b_{3u} 4–10b_{1u} 2–6b_{2g} 2–6b_{3g}.

This model represents the combination of a full target valence CASCI and a rather reduced MRMPS treatment, in which only single excitations out of the Hartree–Fock ground state are considered. Within this general framework, the ideal model is probably model 10 which combines full target valence CASCI and MRMPS configurations based on all possible excitations out of this extended valence space. Unfortunately, this model leads to scattering calculations which are far too big to contemplate at the present time and therefore was not pursued.

We need to choose an optimal model that gives a reasonable-sized target wavefunction expansion as well as good polarizabilities. As shown in table 1, the difference between models 1 and 2 is that there is one more σ_g orbital in the CAS for model 1. This increases the number of target configurations by more than a factor of 3. Model 3 freezes ten electrons in the $1\sigma_g\ 2\sigma_g\ 3\sigma_g\ 1\sigma_u\ 2\sigma_u$ orbitals; it gives a much smaller Hamiltonian matrix ($L = 122$). However, model 3 gives a $^1\Pi_u$ ground state instead of X $^1\Sigma_g$, so was not considered further.

Six electrons were frozen in the core in model 4. The PCO CSFs correspond to the molecular orbital (MO) CSFs, but with one electron put into PCOs from $3\sigma_g\ 4\sigma_g\ 2\sigma_u\ 3\sigma_u\ 1\pi_g$. Model 5 was constructed using the MO CSFs from model 2 and the two PCO CSFs from model 3. This model gives a target Hamiltonian matrix of size 860, which is a fairly good choice for continuing calculations. The MO CSFs for models 6 and 8 are the same as model 5, and several configuration for the PCO CSFs were generated by placing one or two electrons in the $4\sigma_g\ 3\sigma_u\ 1\pi_g$ orbitals. Model 7 places one more σ_g orbital in the CAS compared to model 6. The extra PCO CSFs in model 8 leads to a larger Hamiltonian matrix of dimension 6384 compared to 1511 for model 5. Models 9 and 10 give significantly more configurations than the models designed above.

In order to choose an appropriate model, the polarizabilities for each model were calculated using the sum-over-states method (Jones and Tennyson 2010); the results are shown in table 2. Both $\alpha_\perp$ and $\alpha_\parallel$ of model 3 give rather small values compared to experimental values (Nakagawa 1995). This is because the pure target representation without PCOs does not match that with PCOs. Model 4 gives the biggest polarizabilty among these given models, but it also gives a fairly large target Hamiltonian matrix of dimension 3415.

Table 2. Polarizabilities of C_2H_2 in a_0^3 for the basis of PCOs with $\beta = 1.4$ and $\alpha_0 = 0.17$ for different models. The experimental data are from Nakagawa (1995).

Model	$\alpha_\parallel$	$\alpha_\perp$
1	26.51	15.65
2	26.33	15.67
3	6.78	4.18
4	33.84	15.65
5	26.89	14.88
6	24.37	12.83
7	24.20	12.64
8	27.23	13.82
9	26.87	14.20
10	27.13	13.04
exp.	30.73	18.83

Table 3. Polarizabilities of C_2H_2 for the basis of PCOs with $\beta = 1.4$ and $\alpha_0 = 0.17$ for different MRMPS calculations based on model 5.

Model	$\alpha_\parallel$	$\alpha_\perp$
spd	26.89	14.88
spdf	27.57	13.49
spdfg	27.64	15.26

Given the criteria for choosing an appropriate model, models 4 and 5 were chosen as possible target representations. Model 4 gives the PCOs in the configurations represented as in D_{2h} notation:

5–21a_g 2–8b_{2u} 2–8b_{3u} 1–5b_{3u} 4–10b_{1u} 2–6b_{2g} 2–6b_{3g} for an spd-PCOs calculation;

5–21a_g 2–18b_{2u} 2–18b_{3u} 1–5b_{3u} 4–20b_{1u} 2–6b_{2g} 2–6b_{3g} 1–5a_u for an spdf-PCOs calculation;

5–36a_g 2–18b_{2u} 2–18b_{3u} 1–15b_{3u} 4–20b_{1u} 2–16b_{2g} 2–16b_{3g} 1–5a_u for an spdfg-PCOs calculation.

Polarizabilities for various MRMPS calculations shown in table 3 are performed based on model 5 with $\beta = 1.4$ and $\alpha_0 = 0.17$. Improved polarizabilities for both the parallel component and the perpendicular component are given with the extended PCO basis.

4. Scattering calculation

Scattering calculations were performed starting with a static model. The continuum basis set used to describe the incident positron was taken from Faure *et al* (2002), which gives the continuum orbitals as (9s,7p,7d,7f,6g) for the *R*-matrix radius $a = 10$ a_0. The positron can be placed in all target and continuum orbitals. For the SP model, a number of single-excited target configurations were generated by allowing single excitations of one target electron to a virtual orbital.

For the MRMPS calculation, continuum basis functions with exponents higher than those in the PCO basis for a given ℓ were removed from the basis. The continuum orbital basis actually used in the calculations was (6s,7p,7d,6f,6g) when $\alpha_0 = 0.17$. The deletion threshold for orthogonalizing the continuum orbitals was set to $\delta_{\text{thresh}} = 2 \times 10^{-6}$. The MRMPS expansion was based on target states whose energies are up to about 20 eV above the ground state. We used 42 singlet target states in the close-coupling expansion for the spd-PCOs model, and 64 states for the spdf-PCOs model and spdfg-PCOs models. The CI models used in our calculation can be represented as

$(1\sigma_g\ 1\sigma_u)^4\ (2\sigma_g\ 3\sigma_g\ 4\sigma_g\ 2\sigma_u\ 3\sigma_u\ 1\pi_u\ 1\pi_g)^{10}$ (COs)$^{\mathbf{1}p}$

$(1\sigma_g\ 2\sigma_g\ 3\sigma_g\ 1\sigma_u\ 2\sigma_u)^{10}\ 1\pi_u{}^3$ (PCOs)^1 (COs)$^{\mathbf{1}p}$

$(1\sigma_g\ 2\sigma_g\ 3\sigma_g\ 1\sigma_u\ 2\sigma_u)^{10}\ 1\pi_u{}^2\ (4\sigma_g\ 3\sigma_u\ 1\pi_g)^1$ (PCOs)^1 (COs)$^{\mathbf{1}p}$

and L^2 CSFs:

$(1\sigma_g\ 1\sigma_u)^4\ (2\sigma_g\ 3\sigma_g\ 4\sigma_g\ 2\sigma_u\ 3\sigma_u\ 1\pi_u\ 1\pi_g)^{10}$ (MOs+PCO)$^{\mathbf{1}p}$

$(1\sigma_g\ 2\sigma_g\ 3\sigma_g\ 1\sigma_u\ 2\sigma_u)^{10}\ 1\pi_u{}^3$ (PCOs)^1 (MOs+PCO)$^{\mathbf{1}p}$

$(1\sigma_g\ 2\sigma_g\ 3\sigma_g\ 1\sigma_u\ 2\sigma_u)^{10}\ 1\pi_u{}^2\ (4\sigma_g\ 3\sigma_u\ 1\pi_g)^1$ (PCOs)^1 (MOs+PCO)$^{\mathbf{1}p}$,

where $\mathbf{1}p$ represents the positron which can enter all of the target MOs, even fully occupied ones.

Although we choose models which give fairly small target Hamiltonian matrices, they still give huge Hamiltonians for the scattering calculation. Table 4 illustrates how the size of the scattering Hamiltonian grows rapidly with the model used. The size of the Hamiltonian matrices makes the use of the partitioned *R*-matrix method (Tennyson 2004) essential. The final number of solutions retained from the Hamiltonian matrix is 3000 for all of the MRMPS calculations that we performed.

Table 4. Dimension of the Hamiltonian matrix for scattering calculations for different MRMPS calculations.

	Model 5			Model 4
	spd	spdf	spdfg	spdf
Σ_g^+	521 96	877 11	141 332	524 938
Π_u	502 49	855 44	138 281	521 288
Σ_g^-	493 63	845 88	137 572	490 336
Σ_u^+	518 03	875 93	140 888	502 736
Π_g	508 97	866 02	140 179	499 338
Σ_u^-	493 40	845 40	137 496	494 358

5. Results

The eigenphase sums of Σ_g^+ symmetry for positron–C_2H_2 scattering were calculated using various *R*-matrix models: static, SP and close coupling with MRMPS. For calculations at the static level, the eigenphase is negative, as shown in the upper panel of figure 1. The SP calculation gives a slightly higher eigenphase than the spd-PCOs calculations at energies below 0.3 eV. It passes through zero at about 2.2 eV, which predicts a minimum value of the cross sections for the Σ_g^+ symmetry. The eigenphase sums calculated with the MRMPS method with model 5 (see table 1) show progressively increasing results from the spd-PCOs calculation to the spdfg-PCOs calculation. For calculations with spdfg-PCOs, the eigenphase becomes negative at about 4.2 eV. The upper panel also gives the semi-empirical eigenphase sums calculated by Franz *et al* (2008), whose value with π added, lies above all of our *R*-matrix calculations. However, these eigenphases do not display the correct low-energy behaviour and therefore should probably be regarded as unphysical.

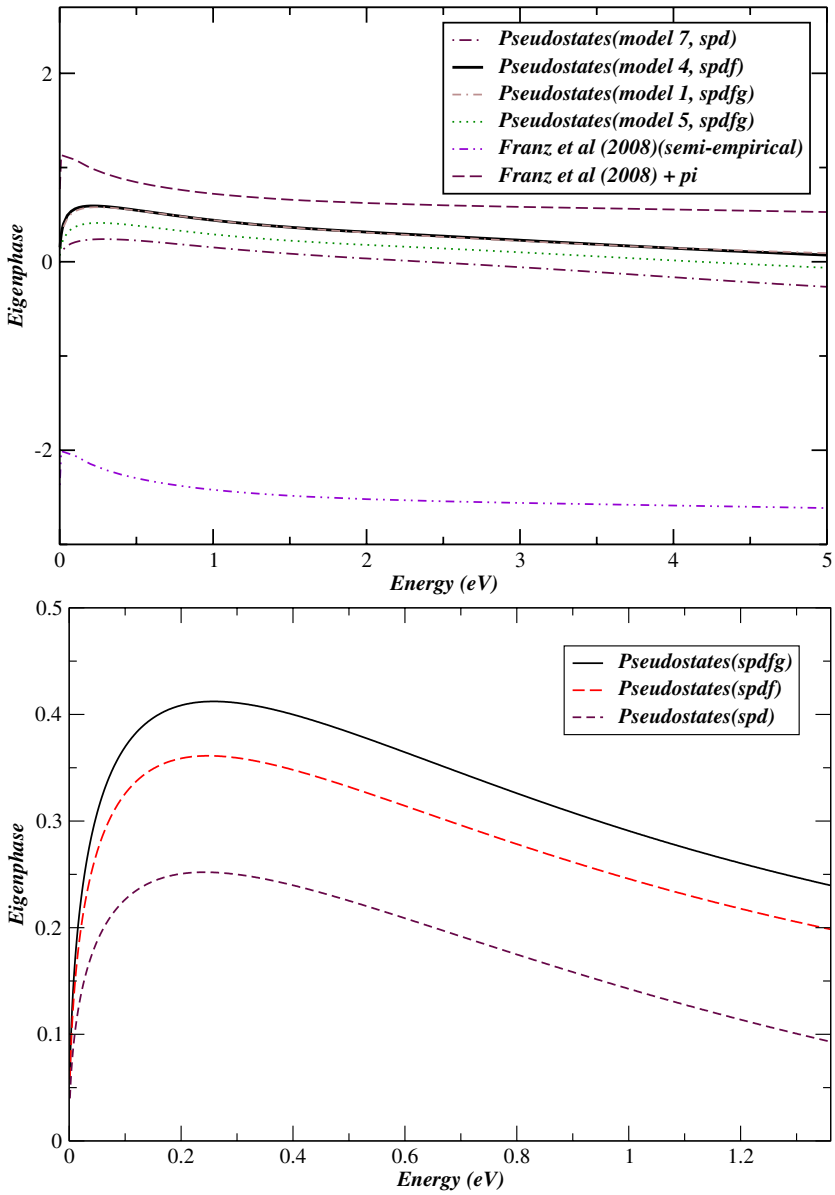

Figure 1. Σ_g^+ symmetry eigenphase sums for different *R*-matrix calculations: upper panel comparison with semi-empirical results; lower panel: model 5 with different PCO basis sets.

The lower panel of figure 1 shows eigenphase sums for the MRMPS calculations and model 5 for collision energies up to 1.3 eV. The results suggest that the eigenphases peak at about 0.22 eV. Figure 2 represents the corresponding total elastic cross sections in $Å^2$ for Σ_g^+ symmetry as a function of energy from different MRMPS calculations. The spdfg-PCOs model gives the largest values at energies below 1.8 eV.

Tests were performed for four models based on A_g symmetry MRMPS calculations, see figure 2. Among these, model 4 with spdf-PCOs gives the best results for the cross sections and exhibits an important improvement for the energies below 2 eV compared to the other models. Furthermore, for model 1, the calculation with spdfg-PCOs gives a significant increment to the spd-PCOs one, particularly at very low energies. Hence, we can expect that model 4 calculations with spdfg-PCOs would give better agreement with the measured cross sections. It is interesting to note that model 4 does not provide the most flexible target representation of those tested, but is the one with the best balance with the pure CASCI and PCO parts of the wavefunction. This observation may provide an important pointer for designing future models.

Figure 3 shows all of our *R*-matrix calculations of integral scattering cross sections below the positronium formation threshold. The static calculation gives lower initial integral cross sections than other models. However, it increases from 0.4 eV. It even lies higher than model 5 with spd-PCOs above 1.8 eV. At near-zero energies, the MRMPS models give higher cross sections than static and SP models. While the most complicated model employed for MRMPS calculations, model 4 with spdf-PCOs gives the highest ICS. These results indicate that the application of the MRMPS method leads to an improved representation of polarization effects for positron collision with acetylene at energies below 5 eV. Comparing

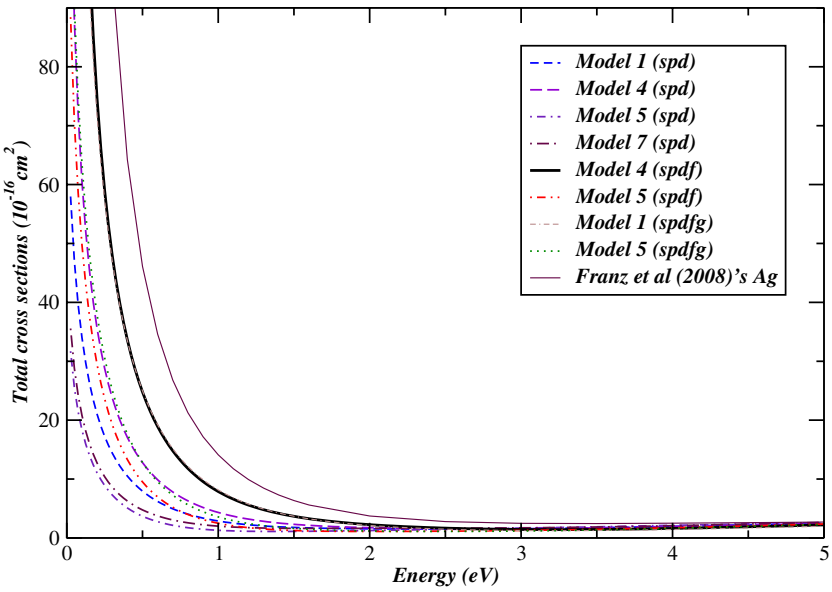

Figure 2. Calculated positron–C_2H_2 total elastic scattering cross sections for Σ_g^+ symmetry corresponding to different MRMPS calculations.

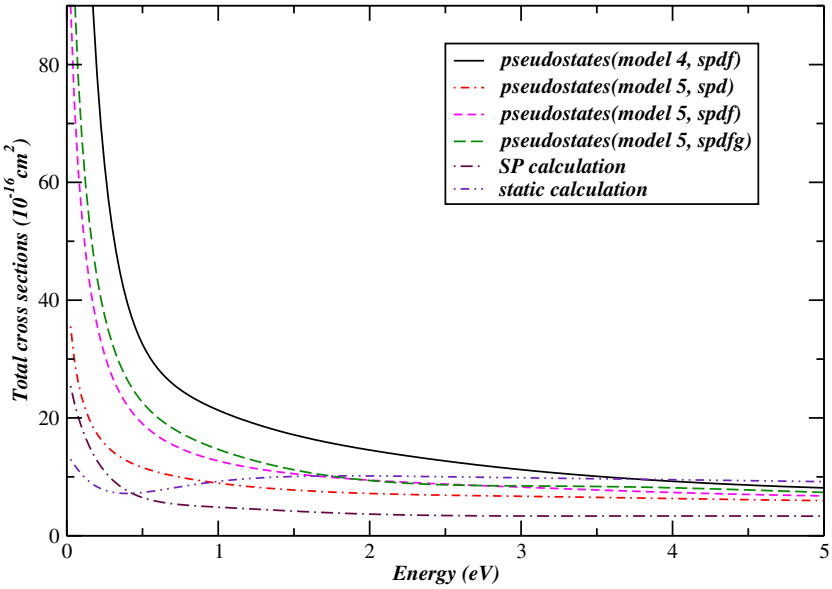

Figure 3. Elastic integral cross sections for positron–C_2H_2 collision using various *R*-matrix models.

with figure 2, the ICS is dominated by the Σ_g^+ symmetry at lower energies.

For positron–C_2H_2 collisions, the cross sections increase rapidly as the scattering energy goes to zero. The scattering length, $a_{\rm scat}$, can be calculated from the s-wave eigenphase. Using the Σ_g^+ eigenphase at 0.001 eV and model 4 (spdf) gives a scattering length, $a_{\rm scat}$, of -12 a_0. We would expect $a_{\rm scat}$ to become even more negative for larger PCO basis sets, although extrapolations using standard formulae (Gribakin and Ludlow 2002, Mitroy and Bromley 2006) suggest that this effect would change $a_{\rm scat}$ by less than 20%. However, the negative scattering length we obtain suggests the presence of a virtual state rather than an s-wave bound state (Taylor 1972).

The s-wave scattering cross sections can be derived by using the formula $\sigma_{\rm sl} = 4\pi\,|a_{\rm scat}|^2$ and compared to the s-wave total elastic cross sections at near zero energy. A scattering length of $a_{\rm scat} = -12$ a_0 gives a low-energy cross section of 1802 a_0^2 which can be compared to our calculated value of 1677 a_0^2, which represents reasonable agreement. However, the scattering length calculations by de Carvalho *et al* (2000a) gives $a_{\rm scat} = -229$ a_0, and by Nishimura and Gianturco (2005) gives $a_{\rm scat} = -90.07$ a_0 for positron collision with C_2H_2. These magnitudes are larger than that we would expect from our calculations.

Comparisons of the calculated elastic integral cross sections from our MRMPS calculation with model 4 spdf-PCOs were made with the experimental measurements of

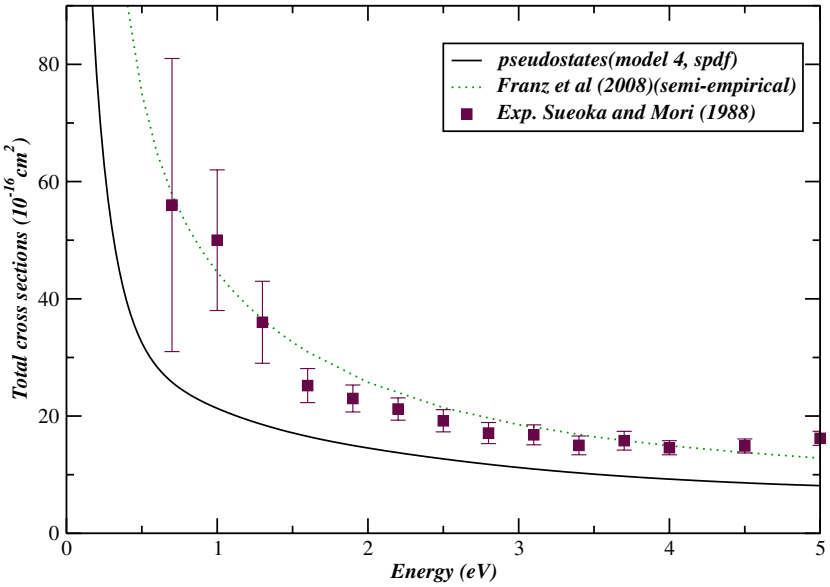

Figure 4. Comparisons of calculated integral cross sections with other theoretical and experimental studies for positron–C_2H_2 scattering at energies below 5 eV.

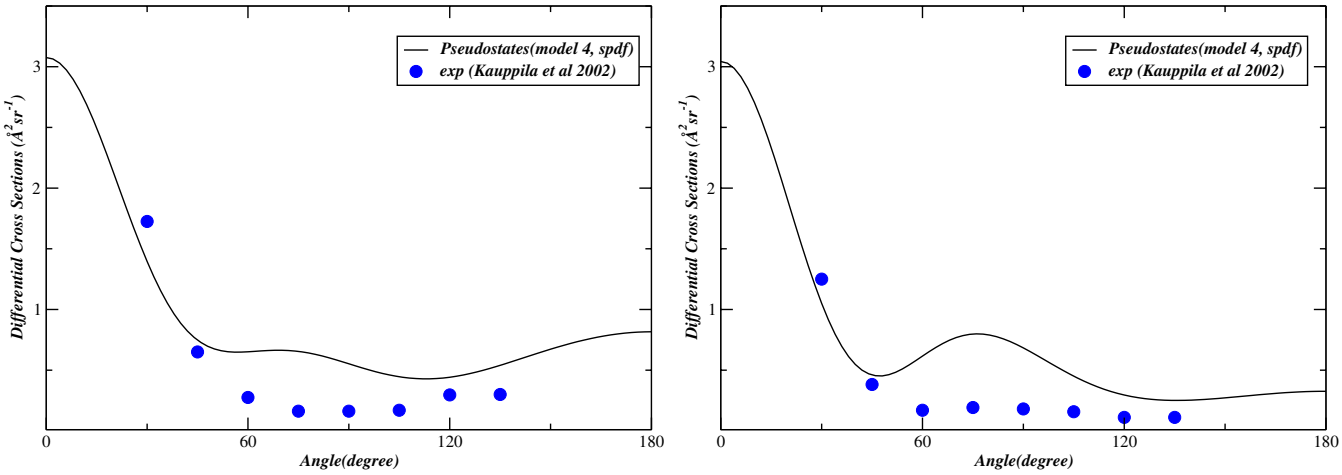

Figure 5. Comparisons of calculated differential cross sections with the measurements of Kauppila *et al* (2002) for positron–C_2H_2 scattering at 4.0 eV (upper panel) and 6.75 eV (lower panel). Note that the measurements are only relative cross sections and the absolute magnitudes of these cross sections therefore refer only to the calculated values.

Sueoka and Mori (1989) and the semi-empirical study of Franz *et al* (2008). Figure 4 shows that Franz *et al* (2008) exhibit good agreement with the experiment. Although our integral cross sections lie lower than the measurement, the MRMPS calculation with spdfg-PCOs or spdfgh-PCOs can be assumed to give higher results than the spdf-PCOs ones shown in figure 4.

Given the low flux of positrons used in most experiments, measurements of positron–molecule differential cross sections (DCSs) are rare. However, Kauppila *et al* (2002) give relative DCS for positron–acetylene collisions at a number of energies. Figure 5 compares our DCSs calculated with model 4 with these measurements for the lowest two energies considered experimentally. In agreement with the observations, and previous calculations (Franz *et al* 2008), the DCS is strongly forward peaked. This behaviour is not found in static or SP calculations. We note that the DCS for electron–acetylene collisions looks markedly different with a strong sideways peak (Kochem *et al* 1985).

6. Conclusions

Elastic integral scattering cross sections for positron–C_2H_2 collisions with pseudo-states up to *g* orbitals are reported and compared to relevant measurements (Sueoka and Mori 1989, Kauppila *et al* 2002) and previous theoretical results (de Carvalho *et al* 2000b, Franz *et al* 2008) at energies below the positronium formation threshold. Our MRMPS method calculations give significantly better results than calculations using static and static plus polarization (SP) models. This suggests that again the MRMPS method gives a better representation of polarization effects at the energies we consider.

However, consistent and complete MRMPS models for many-electron targets lead to Hamiltonians which are unfeasible for us to work with at the present time. Although the choice of a reduced but consistent model is found to give good results, we cannot claim that our calculations are fully converged. Code developments are currently in progress aimed at being able to significantly increase the size of the scattering Hamiltonian that can practically be handled and therefore the complexity of the model used.

Even with the models explored here it is clear that the positron–acetylene system supports a virtual state as suggested by Nishimura and Gianturco (2003). Conversely, we find no evidence that C_2H_2 can bind a positron in its equilibrium geometry. This finding is not necessarily contrary to observation. Firstly, improving our treatment of polarization can only make the virtual state more pronounced and could possibly lead to a bound state. Secondly, the binding energy deduced from the experiment is very small (Young and Surko 2008). Finally, calculations on the well-known virtual state in the electron–CO_2 system have shown (Tennyson and Morgan 1999) that this state becomes bound at bent geometries where extra, dipole attraction is introduced. It is possible that a similar situation occurs for positron–acetylene.

Acknowledgments

The authors thank Edward Armour, Kasturi Baluja, Jan Franz, Gleb Grebakin and Alex Harvey for helpful discussions, and Clara Cassidy for her comments on the manuscript. This work was performed with the support of UK Collaborative Computational Project 2 and EPSRC.

References

Armour E A G, Baker D J and Plummer M 1990 *J. Phys. B: At. Mol. Opt. Phys.* **23** 3057–74
Baluja K, Zhang R, Franz J and Tennyson J 2007 *J. Phys. B: At. Mol. Opt. Phys.* **40** 3515–24
Barnes L, Gilbert S and Surko C 2003 *Phys. Rev.* A **67** 032706
Bartschat K, Hudson E T, Scott M P, Burke P G and Burke V M 1996 *J. Phys. B: At. Mol. Opt. Phys.* **29** 115–23
Burke P G and Berrington K A (ed) 1993 *Atomic and Molecular Processes, an R-Matrix Approach* (Bristol: Institute of Physics Publishing)
Cooper J N, Armour E A G and Plummer M 2008 *J. Phys. B: At. Mol. Opt. Phys.* **41** 245201
da Silva E P, Germano J S E, Lino J L S, de Carvalho C R C, Natalense A P P and Lima M A P 1998 *Nucl. Instrum. Methods Phys. Res.* B **143** 140–8
Danby G and Tennyson J 1991 *J. Phys. B: At. Mol. Opt. Phys.* **24** 3517–29
de Carvalho C R C, Varella M T D, Lima M A P and da Silva E P 2000a *Phys. Rev.* A **68** 062706
de Carvalho C R C, Varella M T D, Lima M A P, da Silva E P and Germano J S E 2000b *Nucl. Instrum. Methods Phys. Res.* B **171** 33–46
Dunning T H Jr 1970 *J. Chem. Phys.* **53** 2823–33
Faure A, Gorfinkiel J D, Morgan L A and Tennyson J 2002 *Comput. Phys. Commun.* **144** 224–41
Franz J, Gianturco F A, Baluja K L, Tennyson J, Carey R, Montuoro R, Lucchese R R, Stoecklin T, Nicholas P and Gibson T L 2008 *Nucl. Instrum. Methods Phys. Res.* B **266** 425–34
Gorfinkiel J D and Tennyson J 2004 *J. Phys. B: At. Mol. Opt. Phys.* **37** L343–50
Gorfinkiel J D and Tennyson J 2005 *J. Phys. B: At. Mol. Opt. Phys.* **38** 1607–22
Gribakin G F and Ludlow J 2002 *J. Phys. B: At. Mol. Opt. Phys.* **35** 339–55
Gribakin G F, Young J A and Surko C M 2010 *Rev. Mod. Phys.* **82** 2557–607
Halmová G, Gorfinkiel J D and Tennyson J 2008 *J. Phys. B: At. Mol. Opt. Phys.* **41** 155201
Halmová G and Tennyson J 2008 *Phys. Rev. Lett.* **100** 213202
Jones M and Tennyson J 2010 *J. Phys. B: At. Mol. Opt. Phys.* **43** 045101
Kauppila W E, Kwan C K, Przybyla D A and Stein T S 2002 *Nucl. Instrum. Methods Phys. Res.* B **192** 162–6
Kochem K H, Sohn W, Jung K, Ehrhardt H and Chang E S 1985 *J. Phys. B: At. Mol. Phys.* **18** 1253–66
Lehoucq R B, Sorensen D C and Yang C 1998 *ARPACK Users' Guide: Solution of Large-Scale Eigenvalue Problems With Implicitly Restarted Arnoldi Methods* (Philadelphia: SIAM)
Mitroy J and Bromley M W J 2006 *Phys. Rev.* A **73** 052712
Morgan L A, Tennyson J and Gillan C J 1998 *Comput. Phys. Commun.* **114** 120–8
Nakagawa S 1995 *Chem. Phys. Lett.* **246** 256–62
Nishimura T and Gianturco F 2003 *Phys. Rev. Lett.* **90** 183201
Nishimura T and Gianturco F A 2005 *Eur. Phys. J.* D **33** 221–4
Paul D A L and Saint-Pierr L 1963 *Phys. Rev. Lett.* **11** 493–6
Sueoka O and Mori S 1989 *J. Phys. B: At. Mol. Opt. Phys.* **22** 963–70
Tarana M and Tennyson J 2008 *J. Phys. B: At. Mol. Opt. Phys.* **41** 205204
Taylor J R (ed) 1972 *Scattering Theory* (New York: Wiley)
Tennyson J 1986 *J. Phys. B: At. Mol. Phys.* **19** 4255–63
Tennyson J 1996 *J. Phys. B: At. Mol. Opt. Phys.* **29** 1817–28
Tennyson J 2004 *J. Phys. B: At. Mol. Opt. Phys.* **37** 1061–71
Tennyson J 2010 *Phys. Rep.* **491** 29–76
Tennyson J and Morgan L A 1999 *Phil. Trans.* A **357** 1161–73
Young J A and Surko C M 2008 *Phys. Rev.* A **78** 032702
Zhang J Y, Mitroy J and Varga R 2009 *Phys. Rev. Lett.* **103** 223202
Zhang R, Baluja K L, Franz J and Tennyson J 2011 *J. Phys. B: At. Mol. Opt. Phys.* **44** 035203